Development of SiC Power Module Structure by Micron-Sized Ag-Paste Sinter Joining on Both Die and Heatsink to Low-Thermal-Resistance and Superior Power Cycling Reliability

Chuantong Chen, *Senior Member, IEEE*, Aiji Suetake, Fupeng Huo, Dongjin Kim, *Member, IEEE*, Zheng Zhang, *Associate Member, IEEE*, Ming-Chun Hsieh, Wanli Li, Naoki Wakasugi, Kazutaka Takeshita, Yoshiji Yamaguchi, Yashima Momose, and Katsuaki Suganuma, *Senior Member, IEEE*

***Abstract*—In this study, the thermal characteristics and structure reliability during power cycling for the four types of SiC power module fabricated using a SiC-heater chip, direct bonded aluminum (DBA) substrate, and aluminum (Al) heatsink were evaluated. Two die-attach materials, including a Sn-Ag-Cu (SAC 305) solder and an Ag paste sinter, were used to bond the SiC to DBA substrate. Furthermore, three types of substrate bonding layers, including SAC solder and Ag paste sinter, and Si grease, were used to bond the DBA substrate to the Al heatsink. The large area bonding between the DBA substrate (30 × 30 mm^2) and Al heatsink was achieved. In addition, compared with the traditional SAC solder-Si grease joint structure, the SiC chip temperature decreased from 265.5 to 180.4 °C and the total thermal resistance of the joint structure decreased from 1.58 to 0.85 K/W for the Ag–Ag sinter joint at the same input power. The heat dissipation improved by 1.86 times. The results were validated and fit well using three-dimensional finite element analysis. The failure time was improved 14.5 times from 2340 cycles to 33 926 cycles for the Ag–Ag sinter joint during the power cycling test. This study will help us to create a SiC power device structure that is smaller, thinner, and possesses ultra-low thermal resistance, and high reliability.**

***Index Terms*—Ag sinter paste joining, direct bonding to Al heatsink, large area bonding, power cycling reliability, SiC die-attach, thermal resistance.**

Manuscript received 14 December 2023; revised 6 March 2024 and 30 April 2024; accepted 26 May 2024. Date of publication 4 June 2024; date of current version 16 July 2024. This work was supported in part by a project (JPNP14004 under Grant 21502156-0) commissioned by the New Energy and Industrial Technology Development Organization (NEDO), in part by JSPS KAKENHI under Grant 22K04243, and in part by JST under Grant JPMJSF23DB. Recommended for publication by Associate Editor K. Sheng. *(Corresponding author: Chuantong Chen.)*

Chuantong Chen, Aiji Suetake, Fupeng Huo, Zheng Zhang, Ming-Chun Hsieh, and Katsuaki Suganuma are with the The Institute of Scientific and Industrial Research (SANKEN), Osaka University, Ibaraki 567-0047, Japan (e-mail: chenchuantong@sanken.osaka-u.ac.jp; asuetake@sanken.osaka-u.ac.jp; huofp@sanken.osaka-u.ac.jp; zhangzheng@sanken.osaka-u.ac.jp; hsieh@sanken.osaka-u.ac.jp; suganuma@sanken.osaka-u.ac.jp).

Dongjin Kim is with the Micro-Joining Center, Korea Institute of Industrial Technology (KITECH), Incheon 21999, South Korea (e-mail: dongjinkim@kitech.re.kr).

Wanli Li is with the Jiangsu Key Lab of Advanced Food Manufacturing Equipment and Technology, School of Mechanical Engineering, Jiangnan University, Wuxi 214122, China (e-mail: li.wanli@jiangnan.edu.cn).

Naoki Wakasugi, Kazutaka Takeshita, Yoshiji Yamaguchi, and Yashima Momose are with the Yamato Scientific Company Ltd., Tokyo 135-0047, Japan (e-mail: naoki.wakasugi@yamato-net.co.jp; kazutaka.takeshita@yamato-net.co.jp; yamaguchiyo@yamato-net.co.jp; yashima.momose@yamato-net.co.jp).

This article has supplementary material provided by the authors and color versions of one or more figures available at https://doi.org/10.1109/TPEL.2024.3408798.

Digital Object Identifier 10.1109/TPEL.2024.3408798

I. Introduction

RECENTLY, it was found that silicon (Si) power semiconductors exhibit high energy losses owing to the significant heat generated during dc/ac power conversion for inverters used in the power supply regulation of high-output motors, such as electric vehicles, hybrid electric vehicles, electric railways, industrial robots. In contrast, dc/ac power conversion based on Si carbide (SiC) power semiconductors offers higher thermal conductivity, higher electron mobility, and lower power losses [1], [2]. The main advantage offered by SiC in power conversion is its low drift region resistance, which is a key factor for high-voltage power applications. The wide band gap and high thermal stability also allow SiC power semiconductors to be used at junction temperatures higher than those of Si, even over 250 °C [3], [4], [5]. Currently, in SiC-SBD or SiC-MOSFET power module structures, SiC power semiconductor chips need to connect to a substrate for primarily electric conduction, thermal dissipation, and structure fixation. In addition, the substrate was bonded to a heatsink for the thermal dissipation. Die attach and substrate bonding are the most important interconnection of the SiC power semiconductors. To meet the high-temperature operation requirement, there is increasing demand for developing die-attach and substrate bonding materials and power module structures that can withstand the high-temperature operation and harsh working environments [6], [7], [8], [9].

Ag nano-paste sinter joining is becoming an important interconnection technology for die attach in SiC power semiconductors. It exhibits superior process ability, high-temperature resistance, and long-time durability to traditional interconnection methods such as solder joining or conductive adhesive joining [10], [11], [12], [13]. Massive works have demonstrated Ag nano-paste sinter joining is capable of achieving a robust and reliable bonding with substrate under sintering temperatures

from 200 °C to 300 °C and in a pressure ranging from 0 to 40 MPa [14], [15], [16], [17]. Ag nano-paste sinter joining offers a good solution for realizing the die attach and has gained increasing attention in SiC power modules for its high-temperature applications. However, Ag nano-paste used Ag nanoparticles tend to aggregate due to the large specific surface area. A protective dispersant is generally required to fabricate the Ag nano-paste [18], [19], [20], [21]. In addition, cost is another issue for Ag nano-paste.

Recently, a kind of Ag hybrid paste consisting of big Ag particles with micron size and small Ag particles with nano or submicron size was introduced [22], [23], [24]. The usage of micron Ag particles can significantly reduce the cost of paste. Meanwhile, the sinter-ability can be guaranteed due to the existing nano or submicron-sized Ag particles. These nano or submicron-sized particles, which can be sintered at a comparatively low temperature, nicely fill in interspaces among micron-sized Ag particles, connecting both big Ag particles and bonding interface. This kind of Ag paste also possesses a preferable density after sintering and thus can offer lower electrical resistance and higher thermal conductivity for die attach. In addition, Ag paste just contains the micron-sized Ag flake particles shows a superior bonding performance even than that Ag hybrid paste [25]. Many researchers have observed in-situ nano-Ag particle generation in micron-sized Ag flake paste [26], [27]. These in-situ nano-Ag particle generation improved the sintering and necking growth in low-temperature pressure-less, which can be attributed to the synergism effect of oxidization and reduction reaction of Ag, and release of micron strain of Ag flake particles [28], [29]. Ag flake particles pasted on different metal metallization layers, such as on Ag, Au, Cu, and Al, exhibited good thermal shock reliability [30], [31], [32], [33].

On the other hand, the thermal management of SiC power module is a big challenge, especially in high-temperature applications. To meet the high-temperature operation requirement, an excellent heat dissipation structure to quickly move the heat generated from the SiC chips is required [34], [35], [36]. Excellent heat dissipation should significantly improve the lifetime of SiC power modules during high-temperature operation. Recently, to solve heat dissipation issue, structure design including Cu clip bonding, Cu pin connection, and novel double-sided or multisided liquid or two-phase flow boiling cooling structures have been developed for SiC power modules [37], [38], [39], [40], [41]. These technologies and structures improved and facilitated to a great extent heat dissipation of SiC power modules. However, regardless of whether it is a single-sided or double-sided structure, the most basic ceramic substrate material such as direct bonded copper (DBC), active metal brazing substrate, or direct bonded aluminum (DBA), and heatsink condenser is necessary in SiC power module [42], [43]. To improve the thermal dissipation performance, both die attach bonding and substrate bonding need to use the materials with a good heat dissipation. Currently, in SiC power modules, Ag paste sinter joining applied for die attach bonding has already developed, but the substrate bonding still uses Pb-free solder or thermal interface material (TIM) grease materials [44], [45], [46]. Because solder and TIM grease possessed a large thermal resistance, leading to heat dissipation and structure reliability issues in SiC power modules.

Recently, large-area bonding by Ag paste sintering has been studied. Although the interface can be achieved to a good bonding with robust shear strength, many voids are still generated at the interface due to organic solvents are difficult to volatilize in a large area [47], [48]. In addition, to get a good bonding with the Ag paste, metallization layers such as electroless plating Ni-P/Ag, Ni-P/Au on both ceramic substrate and heatsink are required. The high-cost metallization process and materials result in serious issues that hinder the Ag nano-paste sinter as a substrate bonding material in the industrial applications. The development of a low-cost Ag paste sinter, metallization-less bonding, as well as a large area bonding technologies will greatly facilitate the application of Ag paste sinter. Furthermore, the thermal resistance and structure reliability evaluation of Ag paste sinter on both die attach, and substrate bonding need to be developed, especially compared with Pb-free solder and TIM grease cases.

In our previous studies, we have reported that DBA is less affected by thermal cycling stress than DBC substrate, owing to the low yield stress of aluminum (Al) [49], [50]. In addition, unlike a DBC substrate, a thin inert alumina (Al_2O_3) layer tightly covers the DBA surface, protecting it from further oxidization. Al was also widely used as a heatsink because Al has some advantages such as low material cost and lightweight. Recently. Ag flake paste was studied, which can be directly bonded to a DBA substrate without Ag or Au metallization layer in a low-temperature pressure-less sintering process [51]. However, the large area bonding of substrate to the heatsink is few reported, and the thermal resistance and structure reliability evaluation for SiC power module using Ag paste sinter as die attach and substrate bonding is never reported.

In this study, a super-low-thermal-resistance SiC power module is proposed using the micron-sized Ag flake paste to join the SiC chip to the DBA substrate as well as to join the DBA substrate to an Al heatsink in low-temperature pressure-less sintering. A Sn-Ag-Cu (SAC) solder and TIM also prepare for the die attach bonding and DBA substrate bonding, the thermal characteristics of the four kinds of joint structure of the SiC/DBA substrate/Al heatsink by different bonding materials were evaluated. In addition, to improve the large area DBA substrate bonding to the Al heatsink, four kinds of sintering profiles were implemented, and the bonding interface was investigated by X-ray image. Finally, the power cycling reliability for the four kinds of power module joints under a high-power density was evaluated. The power cycling reliability of low-thermal-resistance SiC power modules by all Ag paste sinter joining was improved and analyzed in detail. This study provided the design for all interfaces of the SiC/DBA substrate/Al heat sink using an Ag paste sinter in low-temperature pressure-less sintering. It was expected that the Ag paste sinter can eliminate the thermal resistance inside the power module and achieve excellent heat dissipation and power cycling reliability performance. The remainder of this study is structured as follows. Section II presents the materials, joint structure, and bonding process, power cycling experimental details. In Section III, the

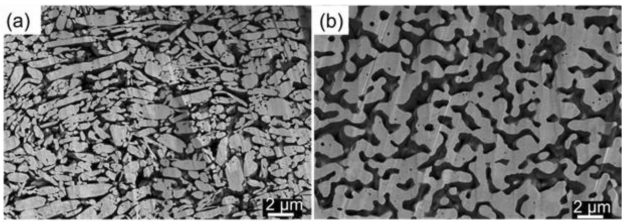

Fig. 1. (a) SEM cross section of micron-sized Ag flake particles. (b) Necking growth and network porous structure after sintering at 250 °C for 5 min in air without assistant pressure.

cross-section of bonded interfaces was observed, and the thermal properties of each module were obtained and analyzed through experiments and three-dimensional (3-D) finite element analyses. In Section IV, power cycling reliability for the four types of SiC/DBA substrate/Al heatsink power module structures is implemented, the on-line thermal resistance is obtained, and the failure time and mechanism are analyzed in detail. Section IV concludes this article.

II. Experiment

A. Solder and Ag Particles Paste

Commercial SAC 305 solder and Si-based thermal interface grease were purchased, whereas micron-sized Ag flake paste was prepared in our laboratory. Only micron-sized Ag flake particles were used as the Ag precursors in the Ag paste. The average size of the Ag particles was 6 μm, and their size distribution can be obtained from our previous studies [52], [53]. CELTOL-IA organic solvent, which can realize Ag flake particle sintering at approximately 180 °C, was used as a solvent. The weight ratio of Ag flake particles and CELTOL-IA organic solvent were mixed to fabricate Ag paste [54], [55], which has a printability with a viscosity of approximately 15 Pa·S at room temperature. Fig. 1(a) shows the SEM cross-section of micron-sized Ag flake particles used in this study. The grain necking growth and network porous structure could be formed at 250 °C for 5 min in the air without assistant pressure as shown in Fig. 1(b).

B. Four Types of Power Module Structures

DBA substrates (Al/AlN/Al) with dimensions of 30 mm × 30 mm × 0.95 mm were prepared. Five island patterns of Al are located at the top. The AlN had a size of 32 mm × 32 mm and a thickness of 0.35 mm [see Fig. 2(a)]. The central part of the DBA, with a size of 6 mm × 6 mm, was bonded to the SiC heater chip. For the Ag paste sinter joining, the surface of the DBA substrate did not undergo any treatment. After Ag paste printing of thickness 100 μm on DBA substrate [see Fig. 2(b)], a SiC heater chip (5 mm × 5 mm × 0.35 mm) was attached to the Ag paste, and the structure was sintered at 250 °C for 30 min in air without assistant pressure [see Fig. 2(c)]. The SiC heater chip is composed of a platinum (Pt) heater wire and a temperature sensor wire, as well as four Au electrodes for the heater wire and sensor on the top surface. After the sintering, the Au wires were bonded to the Au electrodes of SiC heater chip and the DBA substrate [see Fig. 2(d)]. Furthermore, the SAC solder had a thickness of 100 μm to bond with the DBA [see Fig. 2(e)]. The bonding surface of DBA in this case was sputtered by Ti/Ag with thicknesses of 100 nm and 1 μm, respectively. After the SiC heater chip was attached, a reflow process was implemented to bond the SiC heater chip to the DBA substrate [see Fig. 2(f)], and the same Au wires were bonded to the Au electrodes on the SiC heater chip to the DBA substrate as shown in Fig. 2(g). After bonding the SiC chip to DBA substrate, the DBA substrate was then bonded to an Al heatsink using Ag paste, solder, and silicone-based thermal interface grease (G-40M, ShinEtsu) as shown in Fig. 2(h)–(k). We used a metal mask with the thickness of 100 μm to uniformly print the Si grease on Al heatsink. It is the same as the experimental method as the Ag paste printing. The detailed bonding profile for the DBA substrate to Al heatsink will be introduced later.

Fig. 3(a) shows the SEM image of the SiC heater chip which was first coated by the Al_2O_3 layer and then Pt heater wire pattern and Au electrodes. The SiC heater chip was combined with a heater wire and a temperature sensor, both of which were evaporated together by using an electron-beam evaporator process on SiC substrate. The Pt thin film was used as the heater wire, which had a width of 500 μm and a thickness of 200 nm. The Pt probe wire plays the temperature sensor function, which had a width of 100 μm and thickness of 200 nm. If a voltage source is connected across the Pt microheater wire, it results in a current through the circuit. Therefore, the temperature can be measured online by the temperature sensor even with the power ON/OFF switching, which was similar to the power cycling test for the actual power device. The detailed information including dimensions of the SiC heater chip and Pt pattern as well as Au electrodes could be referred to in our previous studies [3], [51], [56]. Fig. 3(b) shows the Au wires bonded on one side Au electrode of the heater wire. The diameter of each Au wire is 45 μm, and there are ten Au wires bonded on each Au electrode. In addition, the detailed sintering of Ag paste and SAC305 reflow profiles for the SiC heater chip bonding to the DBA substrate are shown in Fig. 3(c) and (d), respectively.

For the bonding of the DBA substrate to the Al heatsink using SAC solder, the surfaces of the DBA and Al heatsink to the bonding were sputtered by Ti/Ag with thicknesses of 100 nm and 1 μm, respectively. The reflow profile was the same as introduced in Fig. 3(d). For the Ag-paste sinter joining, no metallization layers were used for the bonding surface of the DBA substrate and Al heatsink. To get a good bonding interface in the large area bonding case, four kinds of different sintering profiles were investigated in advance. The heating rate is set as 20 °C/min, and the difference for the sintering profile is whether there are heating stages at lower temperatures than that sintering temperature as exhibited in Fig. 4(a), (c), and (e). In addition, Fig. 4(g) exhibited the sintering profile with a preheating process, which means that the Ag paste was heated before the DBA substrate was mounted onto the paste. Fig. 4(b), (d), (f), and (h) show the micro focus 3-D computed tomography (CT) X-Ray image of DBA/Al heatsink joint by the four kinds of sintering profile corresponding to Fig. 4(a), (c), (e), and (g), respectively. Interface voids obviously decreased with

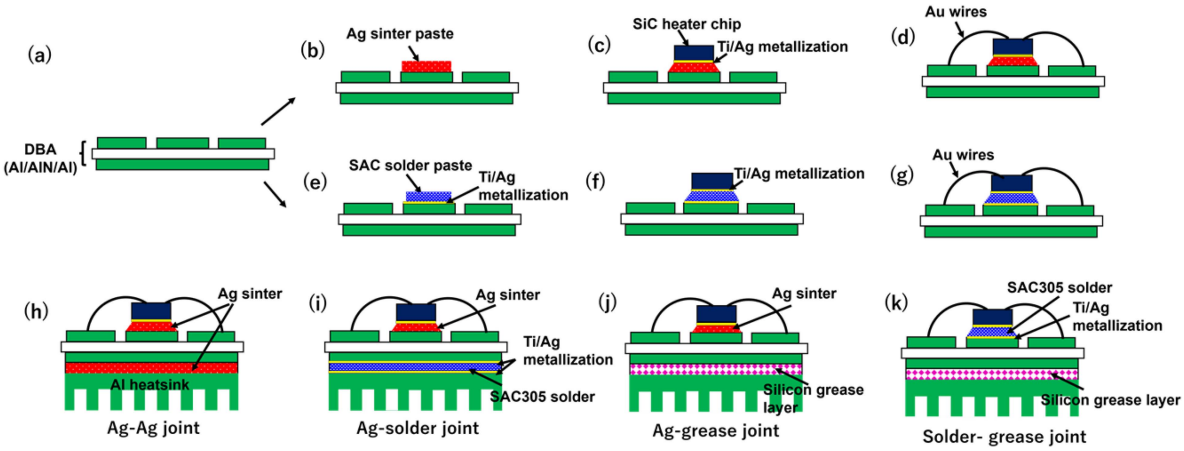

Fig. 2. Schematic diagram of the SiC/DBA/Al heatsink joint structure. (a) DBA substrate preparation. (b) Ag paste sinter printed on the DBA. (c) Sintering after SiC is mounted on the Ag sinter paste. (d) Au wires for SiC to DBA substrate bonding. (e) SAC solder paste printing. (f) Reflow process after SiC chip mounting. (g) Au wire bonding. (h) Bonding DBA with Al heatsink using Ag paste sinter. (i) SAC solder joining. (j) Si grease for DBA bonding with Al heatsink is inserted in the Ag paste sinter die attach structure. (k) Si grease for DBA bonding with Al heatsink is inserted in the SAC solder die attach structure.

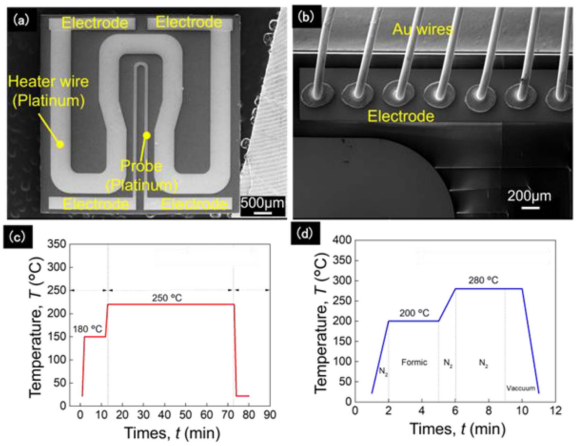

Fig. 3. (a) SEM image of SiC heater chip. (b) Au wires bonded on the electrode. (c) Ag paste sintering profile. (d) Reflow profile of SAC 305 solder for the SiC heater chip bonding to DBA substrate.

TABLE I
FOUR TYPES OF JOINT STRUCTURES USING DIFFERENT BONDING MATERIALS ASSEMBLED FOR DIE ATTACH SIC/DBA AND DBA SUBSTRATE / AL HEATSINK BONDING

Joint structure	*SiC/DBA bonding material*	*DBA/Al heatsink bonding material*
①Ag-Ag joint	Ag sinter paste	Ag sinter paste
②Ag-solder joint	Ag sinter paste	SAC solder paste
③Ag-grease joint	Ag sinter paste	Si grease TIM
④Solder-grease joint	SAC solder paste	Si grease TIM

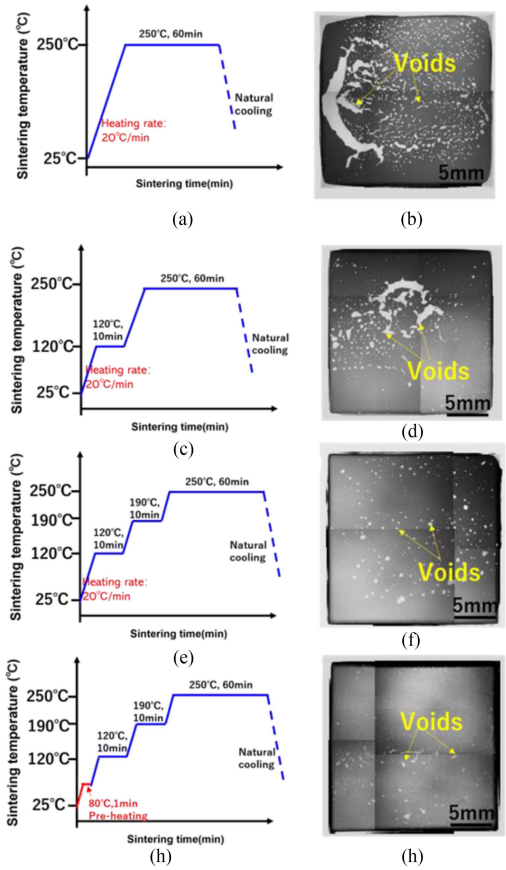

Fig. 4. (a), (c), (e), and (g) Sintering profile without low-temperature stage, with one stage, two stages, and preheating process. (b), (d), (f), and (h) X-ray image of the bonded interface corresponding to the sintering profile of (a), (c), (e), and (g), respectively.

the added heating stage, and the preheating also largely improved the interface bonding quality. In this study, we used the sintering profile of Ag paste shown in Fig. 4(h) for the large area DBA substrate to Al heatsink bonding. For the Si grease, we just apply it evenly on the heatsink surface with the same initial thickness of 100 μm as Ag paste and solder materials.

Table I exhibits the abbreviated names and corresponding bonding materials for the four types of SiC/DBA/Al heatsink joint structures. Fig. 5(a) shows a photograph of Ag–Ag joint, where the SiC heater chip die attach bonding and DBA substrate bonding to the Al heatsink used the Ag paste. Fig. 5(b) shows a tilted and magnified view of the Ag–Ag joint structure.

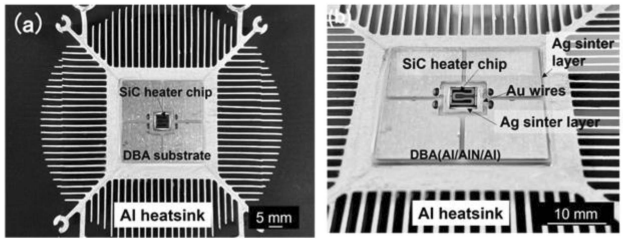

Fig. 5. (a) Photograph of SiC/DBA/Al heatsink power module. (b) Tilted image of the joint structure by all sinter Ag paste joining.

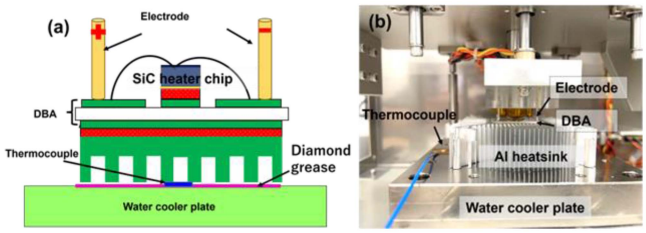

Fig. 6. (a) Schematic diagram of the SiC/DBA/Al heatsink joint structure. (b) Thermal resistance measurement of the SiC/DBA/Al joint.

Together with the other joint structures, which were measured for the thermal resistance and power cycling reliability.

C. Thermal Resistance Measurement

Fig. 6(a) shows a schematic of the joint structure SiC/DBA/Al heat sink, which was placed on a water-cooling plate to measure the thermal resistance. Nanodiamond thermal grease (Ainex, JP-DX1) was applied between the Al heatsink and the water-cooling plate. For the diamond thermal grease, we also used the metal mask with the thickness of 100 μm, and uniformly printed it on the cooling plate. The temperature of the water-cooling plate was set to 25 °C. To make an easy comparison of the SiC chip temperature and thermal resistance differences, the same input voltage (80.5 V) and the current (2.1 A) were set for the four kinds of joint structures. The same input power 162.5 W was implemented for the four kinds of joint structure, with the same high-power density (650 W/cm^2). The heat by the Pt heater wires generated on the SiC heater chip was transferred to the water-cooling system through the DBA substrate and Al heatsink. Because the thermal resistance was measured online by using the SiC heater chip, which refers to time-dependent, the time-dependent thermal resistance $Z_{\rm th}$ behavior can be evaluated using the following equations [57], [58]:

$$\mathrm{Q} = I^2 * R \tag{1}$$

$$Z_{\rm th} = \frac{\Delta T}{Q} \tag{2}$$

where Q [W] is the Joule heat generated by the Pt heater wires on the SiC. I is the current traveling through the Pt heater, and R is the electrical resistance of the Pt heater wire. The temperature difference ΔT can be calculated from the temperature of the SiC heater chip and the temperature of the cooling water plate measured using a thermocouple. Fig. 6(b) shows the SiC/DBA/Al joint structure placed on the water-cooling plate and the electrode input on the SiC heater chip.

TABLE II
POWER CYCLING TEST CONDITIONS FOR EACH JOINT STRUCTURE

Joint structure	Input power (W)	Voltage (V)	Current (I)	SiC chip Power density (W/cm^2)	Junction temperature (ºC)	Cooling temperature (ºC)	Temperature Swing (ºC)
①Ag-Ag joint	180.6	85.4	1.92	722.4	200	25	175
②Ag-solder joint	155.9	82.1	1.9	623.6	200	25	175
③Ag-grease joint	145.8	87.0	1.67	583.2	200	25	175
④ Solder-grease joint	141.2	80.1	1.77	564.8	200	25	175

D. Power Cycling Test

In addition, the power cycling test was implemented for the four kinds of joint samples, to evaluate the thermal resistance, structure reliability, and microstructure evolution. The condition of the power cycling test was switched ON for 2 s and then switched OFF for 5 s, and the junction temperature of the SiC heater chip was switched to 200 °C for the four kinds of joint structure by adjusting the input current (I) and voltage (V). The temperature of the cooling water was controlled to be 25 °C, and thus the swing temperature (ΔT) of the SiC-TEG /Ag sinter /DBA was 175 °C. As each joint structure with different die attach and substrate bonding layers, the current, voltage, and input power (Q) were different to get the same junction temperature of the SiC heater chip. The power cycling test conditions for each joint structure are listed in Table II.

E. Finite Element Simulation Methodology

Thermal simulation was performed to understand the temperature distribution of the SiC/DBA/Al heat sink structure with different bonding layers. A commercial finite element analysis (FEA) solver, ABAQUS, was used for the thermal simulation. The FEM simulation involved steady-state thermal analysis using the materials' properties such as density and thermal conductivity as shown in Table S1. The 3-D finite element model is shown in Fig. 7(a), which includes a SiC heater chip, die attach material, DBA substrate, structural bonding material, and Al heat sink. Fig. 7(b) shows a magnified view of the SiC heater chip. Fig. 7(c) shows the 3-D FEM model for the thermal simulation with the mesh sized, where the total nodes of the meshed model were 1 035 065 and the elements number were 356 100. Fig. 7(d) shows the magnified view of the SiC heater chip, in which the minimum mesh size with the length is 10 μm in this simulation model. The detailed mesh, boundary conditions, and material properties are provided in Supporting Information Fig. S3 and Table S1.

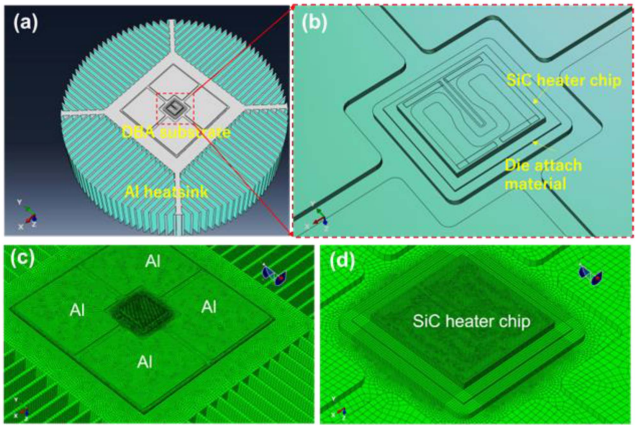

Fig. 7. (a) Three-dimensional finite element model of SiC/DBA/Al heatsink structure. (b) SiC heater chip and die attach model structure.

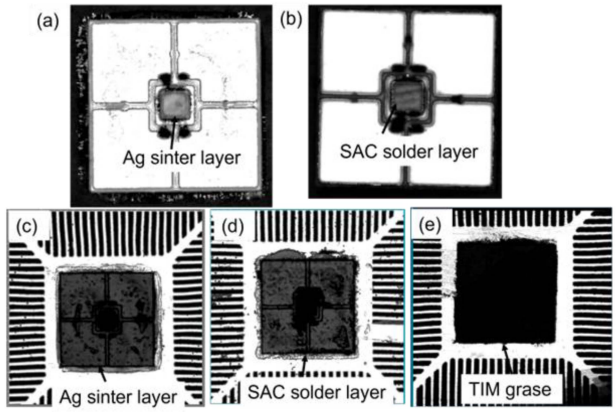

Fig. 8. (a) SAT image of the SiC/DBA/Al heatsink joint structure at the interface of the SiC/DBA by Ag sinter joining. (b) Interface of the SiC/DBA by SAC305 solder. (c)–(e) SAT image of the interface DBA/Al heatsink by Ag sinter joining, SAC solder, and TIM grease, respectively.

F. Characteristic Analysis

The shear strength of the die-attached structure was measured by a shear test, which was performed by using the equipment of a die shear tester (DAGE, XD-7500). The cross-section of the initial joint structure at die attaches bonding and DBA substrate bonding interface was mechanically polished and then fine polished by an ion milling process (IM 4000, HITACHI). The microstructure of the joint structure was observed by Scanning Electron Microscope (SEM, SU8020, Hitachi, Japan). The joint structure before and after the power cycling tests were also observed by Scanning Acoustic Tomography (SAT) and a micro focus 3-D CT X-Ray system (XVA-160N, Uni-Hite System Corporation, Japan). In addition, the bonded interface of sintered Ag and DBA substrate was also observed by Transmission Electron Microscope (TEM, JEM-ARM200F, JEOL) and Energy Dispersive X-ray spectrometry (EDS).

III. Results and Discussion

A. Initial Interface Bonding Observation

Fig. 8(a) and (b) shows the SAT images of the SiC/DBA die attach interface by Ag paste and SAC305 solder joining, respectively. In the case of the Ag paste sinter joining, no large voids were detected, indicating good interface connections. Some patterned structures in the SAC305 solder joining indicated some internal height differences. Cracks or delamination were not observed. Fig. 8(c)–(e) shows the SAT images of the interface DBA/Al heat sink by Ag sinter paste, SAC305 solder, and Si grease, respectively. Some voids still were generated at the interface for the Ag sinter paste and SAC305 solder cases. Void generation can be attributed to solvent evaporation during large-area bonding as introduced in Fig. 4 for the Ag paste sinter joining. For the TIM, no solvent evaporation and defects were observed, and the interface bonding between the DBA and Al heatsink was good.

Fig. 9(a) shows a cross-section of the SiC/DBA die attach joint structure with the Ag paste sinter obtained via scanning electron microscopy (SEM). The sintered Ag paste had a

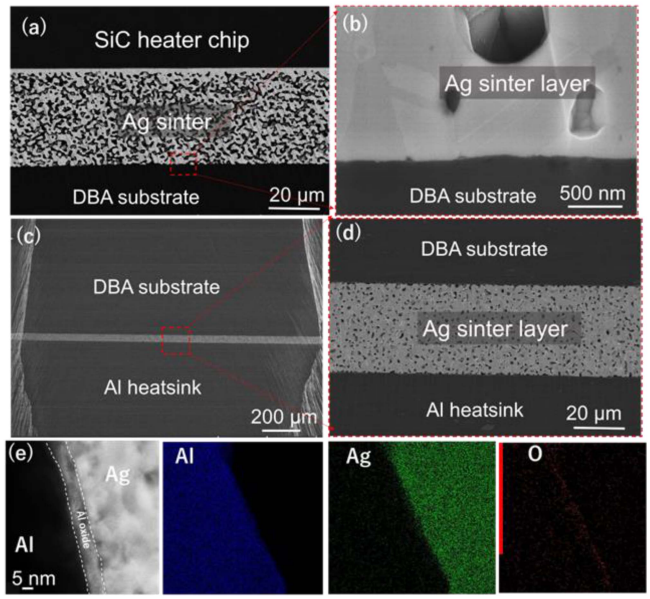

Fig. 9. (a) SEM image of the cross-section of SiC heater chip and DBA substrate by Ag paste sinter and its (b) magnified view at the Ag/Al bonded interface. (c) Cross-section of the DBA substrate and Al heatsink by Ag paste sinter. (d) Magnified view of joint structure. (e) TEM observation of Ag/Al interface and EDS element mapping of Al, Ag, and O.

micron-sized porous network structure without any large voids. Because sintering was implemented in pressure-less, the porosity of the sintered Ag layer was about 40% [59], [60]. Compared with Ag paste sintering in a pressure case, the porosity was larger, which may lead to a relatively small thermal conductivity value. The porosity effect on the thermal resistance and power cycling reliability will be investigated in our further work. Fig. 9(b) shows the bonded interface between the sintered Ag paste and the DBA substrate. The sintered Ag paste was well-bonded to the DBA with strong interface necking growth, indicating that the Ag/Al metal can be bonded together at a significantly low-temperature pressure less. The shear strength for the direct bonding case measured from five samples was

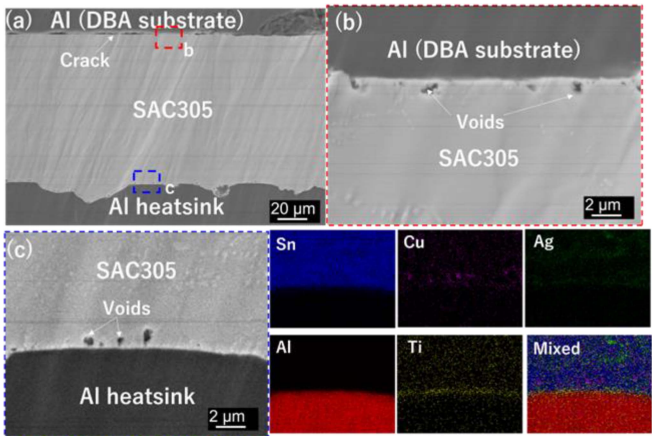

Fig. 10. (a) SEM cross-section of interface DBA/Al heatsink by SAC solder bonding. (b) Magnified view at the DBA/SAC bonded interface. (c) SAC solder /Al heatsink bonded interface and the EDS element mapping.

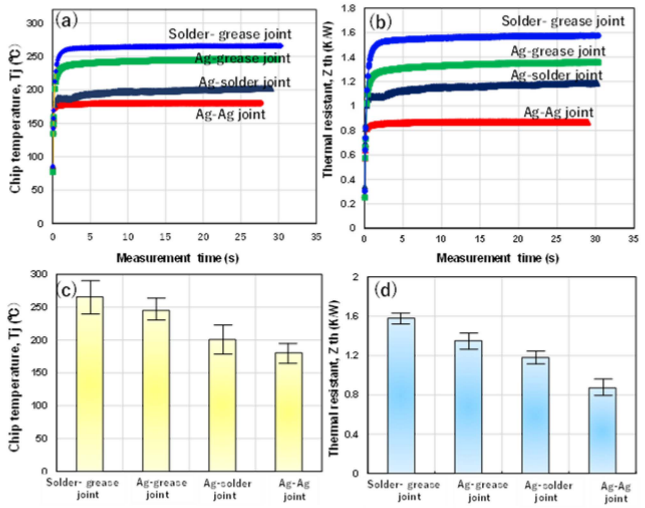

Fig. 11. (a) and (c) Temperature curve and the stabled temperature value of SiC heater chip for the four types of SiC/DBA/Al heatsink structures at the same input power, respectively. (b) and (d) Thermal resistance curve and stabled thermal resistance value of four kinds of the SiC/DBA/Al heat sink structure.

35.9 ± 4.2 MPa, which was larger than that other bonding materials and comparable with Ag paste joining on metallization cases [14], [61]. Fig. 9(c) and (d) shows the SEM image of the cross-section of the DBA/Al heatsink joint structure by Ag paste sinter joining. Since the microstructure of sintered Ag largely depends on the sintering process and the bonding area, the different bonding areas and different sintering processes lead to a different microstructure of sintered Ag including the porosity and pore shape, and the density as shown in Fig. 9(a) and (d). No clear interface delamination or crack generation was observed, including for large-area DBA bonding. The sintered Ag paste was tightly adhered to both the DBA substrate and the Al heatsink. Fig. 9(e) and (f) shows the TEM observations of the Ag/Al interface and EDS element mapping of the bonded interface, respectively. After doing a detailed analysis of the bonded Ag/ Al interface, we confirmed that the sintered Ag diffusion into the Al_2O_3 happened, forming an Ag_2O and Al_2O_3 composite layer with the thickness about 5 nm between Ag and Al. The actual Al_2O_3 layer is very thin, and almost formed with an Ag-O-Al_2O_3 composited layer. The results are like the Ag-Al interface bonding as reported in our previous study [51], [62]. Because the Ag element diffused into the thin Al oxide layer, the layer between sintered Ag and Al is not just a ceramic layer, which is a composited layer with metal Ag, causing electric current to pass through this layer. Therefore, it was thought that the Al oxide layer does not have much effect on the electrical properties of the interface.

Fig. 10(a) shows the initial joint structure of DBA/Al heatsink by SAC solder bonding. No large voids are generated inside the solders, but some cracks and voids can be found at the bonded interface of DBA/SAC solder. Because the bonding area is big, some cracks may be attributed to the warpage occurrence of DBA substrate during the reflow process [63], [64]. Based on the SEM observation as shown in Fig. 10(b) and element mapping (see Fig. S4), intermetallic compound (IMC) did not do so much generated at the bonded interface. For the bonded interface of SAC solder/Al heatsink, the interface voids generation was found but IMC also not so much generated as shown in Fig. 10(c) with the interface element mapping by EDS. On the other hand, although the initial thickness of printed Ag paste and the solder are the same as 100 μm, the thickness of sintered Ag layer changed to thinner with the volatilization of organic solvents and Ag particles necking growth, and finally, the thickness may be slightly thinner than that of the solder layer as shown in Figs. 9(a) and 10(a). Usually, the thicker bonded layer results in a larger thermal resistance. However, because it is very difficult to control the thickness of the sintered Ag layer and solder layer after the fabrication process, especially difficult to get the same thickness, the thickness effect on the thermal resistance was not considered in this study.

B. Initial Thermal Resistance and Temperature Distribution

Fig. 11(a) and (b) shows the temperature curves of the SiC chip surface and the thermal resistance curves after the power-ON state for the four types of SiC/DBA /Al heatsink joint structures at the same input power, respectively. To achieve a stable state of SiC heater chip surface temperature, the input power time was necessary above 25 s. The SiC surface temperature was approximately 180.4 °C for the Ag–Ag joint and 265.5 °C for the solder-grease joint as shown in Fig. 11(c). From the solder-grease to the Ag–Ag joint, the temperature at the SiC surface decreased by 32.1%. In addition, the SiC surface temperature of the Ag-solder joint was 200.1 °C which was lower than that of the Ag-grease joint of 245.1 °C. These results clearly revealed that the thermal dissipation of joint structure largely depends on used bonding material at both die attach and substrate bonding. In addition, the total thermal resistance Z_{th} of the joint structure can be calculated for the four kinds of joint structure as shown in Fig. 11(d). Thermal resistance Z_{th} decreased from 1.58 to 0.85 K/W when the solder-grease joint changed to the Ag–Ag joint. The total thermal resistance decreased by 46.2%, suggesting that the function of heat dissipation improved by 1.8

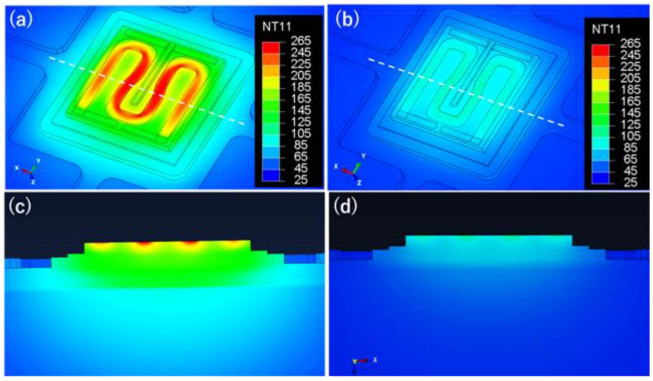

Fig. 12. (a) and (b) Temperature distribution by FEA for the solder-grease and Ag–Ag paste sinter joining. (c) and (d) Temperature distribution in the vertical direction for the two cases joint, respectively.

times. Similar to the SiC chip temperature, the thermal resistance of the Ag-solder joint was lower than that of the Ag-grease joint but larger than that of the Ag–Ag joint. The error bars shown in Fig. 11(c) and (d) were obtained by three samples for each joint structure.

Fig. 12(a) and (b) exhibits the temperature distribution of SiC heater chip in the SiC/DBA /Al heatsink joint structure by solder-grease bonding and Ag–Ag paste sinter joining by 3D FEA, respectively. Like the results obtained from the experiment, the temperature of the SiC heater chip exhibited a significant difference for the solder-grease joint and Ag–Ag joint structure. The maximum temperature occurred at the Pt heater wire was about 265 °C for the solder-grease joint and about 190 °C for the Ag–Ag joint. Fig. 12(c) and (d) shows the temperature distribution in the vertical direction for the solder-grease joint and Ag–Ag joint, respectively. The temperature spreads downward from the SiC heater chip to the Al heatsink. The temperature at the die attach bonding and substrate bonding parts are different, where the Ag–Ag joint was significantly smaller than the solder-grease joint. The results revealed that the heat dissipation of the SiC power module could be significantly improved by using the die attach material and substrate bonding material with better thermal conductivity.

C. Lifetime of Joint Structure During Power Cycling

Fig. 13(a) shows the chip temperature change during the power cycling test for the four kinds of SiC/DBA /Al heatsink joint structures. Although the junction temperature of the SiC heater chip was set as same to 200 °C for the four kinds of joint structure, the evolution of temperature during the power cycling is totally different. The temperature increased quickly to 350 °C after 2340 cycles for the solder-grease joint but keeping the chip temperature of 200 °C to about 30 000 cycles in the case of Ag–Ag joint structure. The failure of solder-grease joint, sinter Ag-grease joint, Ag-solder joint, and Ag-Ag joint were happened after 2340 cycles, 9460 cycles, 16 614 cycles, and 33 926 cycles, respectively. The failure of the joint structure significantly depends on the used die attach materials and substrate bonding materials. Compared with the traditional solder-grease

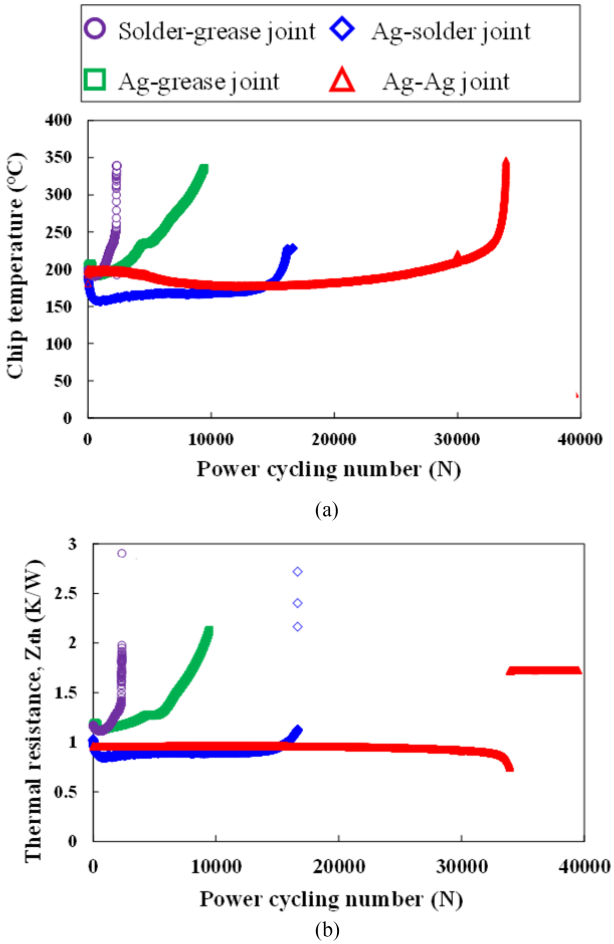

Fig. 13. (a) SiC heater chip temperature change for the four types of SiC/DBA substrate/Al heatsink structures during the power cycling. (b) Thermal resistance change of the SiC/DBA substrate/Al heat sink structure during the power cycling.

joint, the lifetime to failure of Ag–Ag joint structure improved by 14.5 times at the same junction temperature of 200 °C. In addition, compared with the Ag-solder joint, the lifetime to the failure of Ag–Ag joint improved by 2.04 times. The extended life span beyond expectations confirms the advantages of the Ag–Ag joint structure applied in high temperature and harsh environments. On the other hand, the chip temperature of the Ag-solder joint and Ag–Ag sinter joint decreases at the initial stage during the power cycle as shown in Fig. 13(a). We think about the reasons that may be attributed to the resintering of the sintered Ag layer because the sintered Ag can be resintered during a high-temperature aging process, leading to a better interface bonding and a denser structure of sintered Ag layer induced by Ag grain necking growth [65], [66]. Ag resintered process should lead to the thermal resistance decrease and thus decrease the chip temperature at the initial power cycling test. However, with the power cycling number increase, the accumulated thermal stress and strain would lead to the interface cracks generation and thus increase the interface thermal resistance. In addition, for the Ag-solder joint, there are some cracks generated at the solder interfaces after the reflowing process as shown in Fig. 10(a). At the initial stage of power cycling, because of the thermal

expansion of solder and substrate materials, the interface may be touched together at the crack locations, leading to interface thermal resistance decrease and chip temperature decrease.

Fig. 13(b) shows the thermal resistance evolution of the four kinds of SiC/DBA /Al heatsink joint structure during the power cycling test. Similar to the change of chip surface temperature, the thermal resistance evolution also depends on the die attach materials and substrate bonding materials. The Ag–Ag joint exhibits the lowest thermal resistance at initial and a stable thermal resistance during the power cycling to 30 000 cycles. Although the junction temperature of the four kinds of joint structure was set as same, the sintered Ag layer has a far better thermal conductivity than that of solder and grease, leading to a lower thermal resistance and longer lifetime to failure for the Ag–Ag joint case during the power cycling. In addition, the results also suggested that the direct bonding on DBA and Al heatsink by Ag sinter joining possessed a very excellent power cycling reliability, even the DBA substrate/ Al heatsink with a large area bonding. The reason for this failure for each joint structure will be analyzed in the following section.

D. *Failure Analysis of Joint Structure*

Based on the results of Fig. 13, the lifetime to failure can be significantly improved by 14.5 times by changing the die attach and substrate bonding materials from solder and Si grease to Ag sinter joining. The chip temperature and thermal resistance increased during the power cycling for each joint, especially near the failure. The failure should be attributed to the deterioration of the joint structure including bonding layers, DBA substrate, SiC heater chip as well as Au bonding wire. Fig. 14 shows the surface of the SiC heater after the failure of the four kinds of joint structure during power cycles. The local Pt heater wire completely burned, and its failure caused the exposure of the Al_2O_3 layer on the SiC surface for the solder-grease joint, sinter Ag-grease joint, and Ag-solder joint as shown in Fig. 14(a)–(c), respectively. The increase in the measured temperature was mainly caused by the damage or generation of cracks in the heater wire during power cycling.

The reasons for Pt heater wire burn should be attributed to the increased temperature of SiC chip surface during the power cycling. In addition, the Au wires connected from chip electrode to the DBA substrate did not appear clearly breakage and damage in these three joint cases. The temperature increase of the chip surface may be mainly induced by the deterioration of die attach bonding layer or substrate bonding layer. On the other hand, for Ag–Ag joint, the Au wires clearly melted and burned with the electrodes of heater wire, suggesting the joint failure may be induced by Au wire failure at first. Generally, the damage of the wire bonding proceeded from a tiny crack, which can propagate with time due to the cyclic thermal stress, fatigue, and bonding interface delamination [67], [68], [69].

Since the die attaches layer possessed a higher temperature and swing temperature than that substrate bonding layer, leading to larger thermal stress, the formations of cracks and voids in the SiC die attach layer after power cycling test were observed via nondestructive inspection employing a microfocus 3-D CT X-Ray system. Fig. 15(a) shows the X-Ray CT image of the

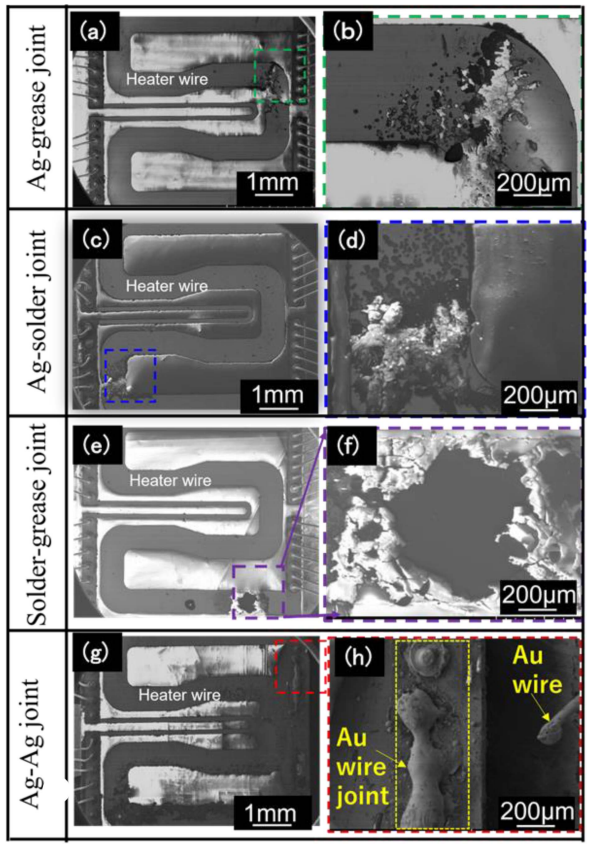

Fig. 14. (a), (c), (e), and (g) SEM image of SiC heater chip surface of the Ag-grease joint, Ag-solder joint, solder-grease joint and Ag-Ag joint after power cycling test, respectively. (b), (d), (f), and (h) Failure location of heater wire and Au wires corresponding to (a), (c), (e), and (g), respectively.

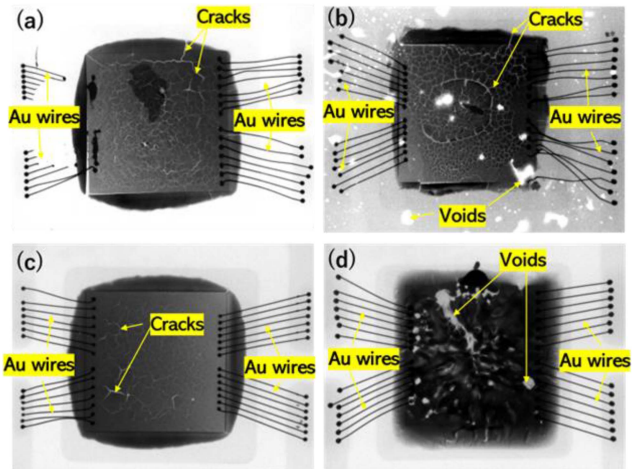

Fig. 15. X-Ray CT image of the (a) Ag–Ag joint, (b) Ag-solder joint, (c) Ag-grease joint, and (d) solder-grease joint structure after power cycling test.

Ag–Ag joint after power cycling. Many cracks appeared and a reticulated distribution was observed in the die attach sintered Ag layer. Cracks also appeared in the sintered Ag layer outside the SiC heater chip. Normally, the cracks could reduce the thermal conduction of the sintered Ag layer, making the temperature of the SiC heater chip increase with the cacks growth. In addition, it was also clearly found that the Au wires were disconnected and

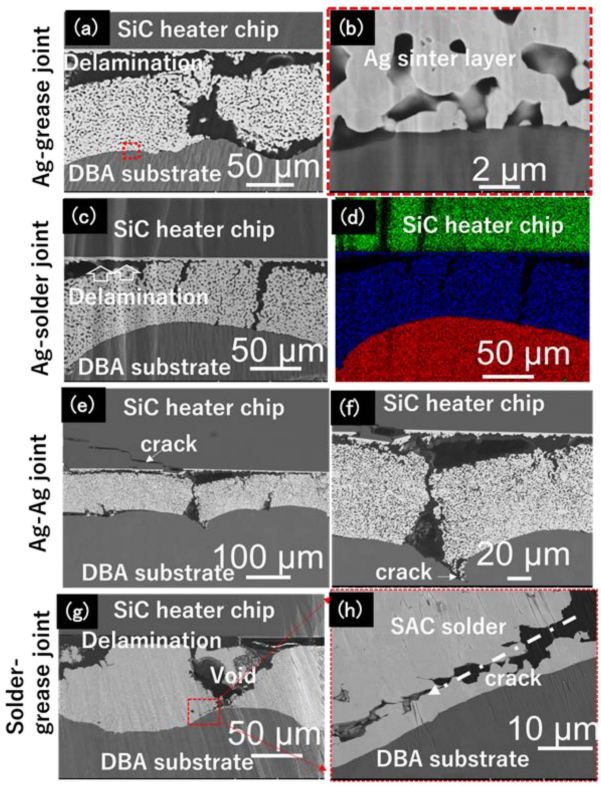

Fig. 16. Cross-sectional SEM image of the four kinds of SiC/DBA/Al heatsink joint structure after power cycling test at die attach part. (a), (c), (e), and (g) Ag-grease joint, Ag-solder joint, Ag-Ag joint, and solder-grease joint structures, respectively. (b), (d), (f), and (h) Local magnified view or EDS element mapping corresponding to (a), (c), (e), and (g), respectively.

failed on the electrode of Pt heater wires. Fig. 15(b)–(d) shows the X-Ray CT image of Ag-solder joint, sinter Ag-grease joint, and the solder-grease joint after the joint was a failure during the power cycling, respectively. Many cracks were generated in the sintered Ag layer with a reticulated distribution for the Ag-solder joint. Many white dots could be found in the Ag-solder joint under the SiC heater chip and outside the chip, which may be the voids generated at the substrate bonding layer. The detailed information will be interpreted by the SEM cross-section observation and shown in Section III-E. For the Ag-grease joint, because the failure happened after 9460 cycles, earlier than that Ag–Ag joint (33 926 cycles) and Ag-solder joint (16 614 cycles), the cracks density generated at the die attach sintered Ag layer was decreased than the other two cases.

E. Cross Section of Joint Structure After Power Cycling

Fig. 16 shows the cross-sectional SEM image of the four kinds of SiC/DBA/Al heatsink joint structures after the power cycling test at die attach the part. Fig. 16(a), (c), and (e) exhibits the Ag-grease joint, Ag-solder joint, and Ag–Ag joint structures, respectively. As the three kinds of the joint structure failed after 9460 cycles, 16 614 cycles, and 33 926 cycles, respectively, the corresponding microstructure evolution of the sintered Ag layer was different. For the Ag-grease joint, the microstructure of sintered Ag layer from a uniform porous structure transforms to a coarser and fractured one with some huge cracks in the vertical direction. The coarsening of the microstructure is attributed to the effect of thermal migration of Ag and oxygen effect during the power cycling process [70], [71]. The cracks generation is due to the thermal stress caused by the coefficient of thermal expansion (CTE) mismatch among the SiC chip, sintered Ag layer, and DBA substrate, which results in the sintered Ag layer to endure tensile and compressive stresses during power cycling [72], [73]. The delamination also happened on the interface between SiC and sintered Ag, as well as the interface between sintered Ag and DBA substrate. The interface delamination is the final state that should be included in the initial interface crack generation, and crack extension. It means that the interface cannot be subjected to the interface thermal stress when the interface delamination happens. The interface delamination generation should significantly influence the thermal dissipation from the SiC heater chip to the heatsink, leading to the heater chip temperature increase and finally failure within a short time.

On the other hand, the sintered Ag still bonded well with DBA substrate at some locations as shown in Fig. 16(b). For the Ag-solder joint, more cracks were generated in the vertical direction also horizontal direction with an interface delamination. The vertical crack generation was discussed in our previous study [74], which was induced by CTE mismatch between sintered Ag and SiC chips. The stress will concentrate at the grain boundaries of the Al layer, and stress gradient will be generated between the Al grain boundary and the inside of the grain, leading to the hillock-like deformation. The porous networks of the sintered Ag layer are partially broken in the vertical direction by this deformation and completely open with the stress gradient of the sintered Ag layer. The DBA substrate undergoes severe plastic deformation because of the low yield strength of Al and the effects of reciprocating thermal stress during the power cycling process. The Ag sintered neck remains tightly bonded to Al with no observable gaps despite Al undergoing severe deformation. After the power cycling test, the Ag and Al interfaces did not seem to inter-diffuse each other as shown in the EDS mapping as shown in Fig. 16(d), that may be attributed to the existence of a thin Al oxide layer between Ag and Al. The Al oxide element was not detected in the sintered Ag layer and DBA because it was very thin less than 5 nm [51]. The sintered Ag layer of Ag–Ag joint also exhibits a similar phenomenon as Ag-solder joint. However, because the thermal conductivity of substrate bonding materials for the Ag–Ag joint, was far better than that the other joints, the heat generated from the SiC chip was more quickly dissipated to heatsink, leading to a lower temperature at the die attach the part. Therefore, the Ag–Ag joint experienced a low-stress, long-term fatigue failure mode, leading to the crack size being smaller than that of the two other joints but possessing the highest crack density as also shown in Fig. 15. In addition, it was also found that crack generated in the SiC heater chip. SiC crack occurrence should be induced by the thermal stress accumulation process. When the energy of thermal strain and stress is larger than that of SiC fracture toughness, the crack will be generated. DBA deformation may increase the thermal stress and crack generation of the sintered Ag layer, resulting in a huge stress concentrated at the bonded interface with SiC. These

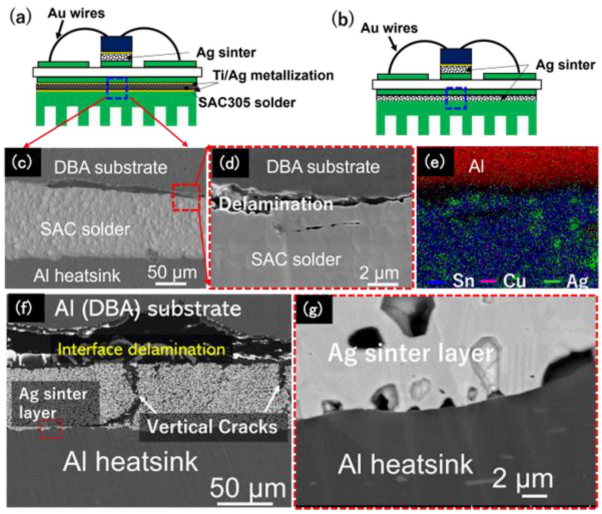

Fig. 17. Image of analyzed part of the bonded layer for DBA substrate to the heatsink of (a) Ag-solder joint and (b) Ag-Ag joint. (c)–(e) SEM image of solder layer and the bonded interface between DBA and SAC solder, the EDS element mapping, respectively. (f) and (g) Joint of DBA substrate by Ag sinter after power cycling and the magnified view of the interface between Ag sinter layer and Al heatsink.

results suggested that the direct bonding of Ag sinter joining on the DBA substrate needs to protect the deformation of the Al surface during harsh operation environment. Further study will investigate the joint structure using the DBC substrate or using the DBA substrate with a thick Ni-P/Ag metallization layer to suppress the deformation and thus improve the joint reliability during power cycling [75], [76].

Fig. 16(g) exhibits the solder-grease joint at the die attach part. Although the solder-grease joint structure was failure after 2340 cycles much shorter than that Ag sinter joint structure, the IMC and void generation for the SAC die attached layer. Large cracks, voids, and interface delamination are generated at the interface between the solder and SiC heater chip. In addition, the huge deformation of the DBA substrate also happened in this case, which may be attributed to the increased temperature and thermal stress during the power cycling. The interface delamination may be first induced by the IMC and interface voids, and the DBA substrate deformation as shown in Fig. 16(h). The IMC and interface delamination hindered the heat dissipation during the power cycling test, and finally resulted in the SiC heater chip temperature increase and heater wire failure in a short time [77], [78].

In this study, we also analyzed the microstructure of substrate bonding for DBA substrate to Al heatsink for the Ag-solder joint and Ag–Ag joint structures after power cycling. We analyzed the central part of the bonded layer for the DBA substrate to heatsink under the SiC chip as shown in Fig. 17(a) and (b), in which the temperature should be higher than that edge part during the power cycling test. Fig. 17(c) shows the SEM cross-section of the Ag-solder joint at the DBA substrate bonding part after the power cycling test. It was found that interface delamination was also generated at the interface between the DBA and SAC solder layer, especially nearly the bonded interface. Comparing the solder-grease joint at the die attach part, the DBA substrate bonding part was subjected a low temperature but a longer power cycling number, and thus the interface delamination generation. The IMC layer did not so much seriously generate at the interface between DBA and SAC solder as shown in Fig. 17(d) and the mixed element mapping [see Fig. 17(e)]. Fig. 17(f) shows the SEM cross-section of Ag–Ag joint at the DBA substrate bonding part after the power cycling test. It was found that the interface delamination also generated at the interface between DBA and the sintered Ag layer, especially near the bonded interface. The vertical cracks generated in the sintered Ag layer and DBA appeared a large deformation similar to the die attach part. On the other hand, except for some crack locations, most of the interfaces between the sintered Ag and Al heatsink are still well bonded as shown in Fig. 17(g). This result suggested that the direct bonding of Ag sinter paste to Al heatsink is a feasible solution that not only saves cost and time but also has high reliability.

IV. Conclusion

This study performed low-temperature low-pressure Ag paste sinter joining (die attach and TIM bonding to Al heat sink) inside a power module without metalizing any bonding interface. Although Ag has a good thermal conductivity, the superior power cycling reliability of joint structure should be based on the good die attach bonding and large area substrate bonding. The preheating and staged-sintering profile of Ag paste for larger area bonding confirmed that it can decrease the interface void generation and largely improve the interface bonding quality. SiC and DBA substrates or DBA substrates and Al heat sinks can be directly bonded to each other, resulting in a remarkable heat dissipation of 1.8 times or more compared with conventional solder and grease bonding structures. The results were validated and fit well using 3-D FEA. In addition, with the same junction temperature, the failure time of conventional solder and grease bonding structures was 2340 cycles, which was improved by 14.5 times to 33 926 cycles for the all-Ag sinter paste structures during the power cycling test. In addition, compared with the Ag-solder joint, the lifetime to failure of Ag–Ag joint improved by 2.04 times. The extended life confirms the advantages of the Ag–Ag joint structure applied in high temperatures and harsh environments.

As a result, Ag paste sinter joining eliminates the requirement for a metalized layer on the substrate surface, making it possible to significantly reduce the costs for electrical device manufacturers and manufacturing processes. Because the DBA substrate and Al heatsink can be directly bonded by Ag paste sinter joining, the DBC, DBA substrate, and metal base plate in the current power module structure are joined by brazing or TIM grease, which may no longer required, making it possible to create a SiC power device structure that is smaller, thinner, and possesses ultra-low thermal resistance. In addition, after the power cycling test, some SEM cross-section results suggested that the direct bonding of Ag sinter joining on the DBA substrate needs to protect the deformation of the Al surface during harsh operation environments. The joint structure using the DBC

substrate or using the DBA substrate with a thick Ni-P/Ag metallization layer to suppress the surface deformation of the substrate may be necessary to further improve the joint reliability during power cycling.

REFERENCES

[1] H. Lee, V. Smet, and R. Tummala, "A review of SiC power module packaging technologies: Challenges, advances, and emerging issues," *IEEE J. Emerg. Sel. Topics Power Electron.*, vol. 8, no. 1, pp. 239–255, Mar. 2020.

[2] J. O. Gonzalez, R. Wu, S. Jahdi, and O. Alatise, "Performance and reliability review of 650 V and 900 V silicon and SiC Devices: MOSFETs, cascode JFETs and IGBTs," *IEEE Trans. Ind. Electron.*, vol. 67, no. 9, pp. 7375–7385, Sep. 2020.

[3] D. Kim et al., "Online thermal resistance and reliability characteristic monitoring of power modules with Ag sinter joining and Pb, Pb-free solders during power cycling test by SiC TEG chip," *IEEE Trans. Power Electron.*, vol. 36, no. 5, pp. 4977–4990, May 2021.

[4] A. Tsibizov, I. Kovačević-Badstübner, B. Kakarla, and U. Grossner, "Accurate temperature estimation of SiC power mosfets under extreme operating conditions," *IEEE Trans. Power Electron.*, vol. 35, no. 2, pp. 1855–1865, Feb. 2020.

[5] N. Murayama, M. S. K.Hirao, T. Tsuchiya, and H. Yamaguchi, "High-temperature electro-ceramics and their application to SiC power modules," *Ceramics Int.*, vol. 44, no. 4, pp. 3523–3530, 2018.

[6] R. Wang, Z. Chen, D. Boroyevich, L. Jiang, Y. Yao, and K. Rajashekara, "A novel hybrid packaging structure for high-temperature SiC power modules," *IEEE Trans. Ind. Appl.*, vol. 49, no. 4, pp. 1609–1618, Jul./Aug. 2013.

[7] F. Hou et al., "Review of packaging schemes for power module," *IEEE J. Emerg. Sel. Topics Power Electron.*, vol. 8, no. 1, pp. 223–238, Mar. 2020.

[8] P. Ning, F. Wang, and K. D. T. Ngo, "High-temperature SiC power module electrical evaluation procedure," *IEEE Trans. Power Electron.*, vol. 26, no. 11, pp. 3079–3083, Nov. 2011.

[9] C. Chen, F. Luo, and Y. Kang, "A review of SiC power module packaging: Layout, material system and integration," *CPSS Trans. Power Electron. Appl.*, vol. 2, no. 3, pp. 170–186, Sep. 2017.

[10] F. Yang, W. Zhu, W. Wu, H. Ji, C. Hang, and M. Li, "Microstructural evolution and degradation mechanism of SiC–Cu chip attachment using sintered nano-Ag paste during high-temperature ageing," *J. Alloys Compounds*, vol. 846, 2020, Art. no. 156442.

[11] H. Zheng, D. Berry, K. D. T. Ngo, and G.-Q. Lu, "Chip-bonding on copper by pressureless sintering of nanosilver paste under controlled atmosphere," *IEEE Trans. Compon., Packag. Manuf. Technol.*, vol. 4, no. 3, pp. 377–384, Mar. 2014.

[12] S. Fu, Y. Mei, X. Li, C. Ma, and G.-Q. Lu, "Reliability evaluation of multichip phase-leg IGBT modules using pressureless sintering of nanosilver paste by power cycling tests," *IEEE Trans. Power Electron.*, vol. 32, no. 8, pp. 6049–6058, Aug. 2017.

[13] F. Yu, R. W. Johnson, and M. C. Hamilton, "Pressureless sintering of microscale silver paste for 300 °C applications," *IEEE Trans. Compon., Packag. Manuf. Technol.*, vol. 5, no. 9, pp. 1258–1264, Sep. 2015.

[14] R. Khazaka, L. Mendizabal, and D. Henry, "Review on joint shear strength of nano-silver paste and its long-term high temperature reliability," *J. Electron. Mater.*, vol. 43, no. 7, pp. 2459–2466, 2014.

[15] T. F. Chen and K. S. Siow, "Comparing the mechanical and thermal-electrical properties of sintered copper (Cu) and sintered silver (Ag) joints," *J. Alloys Compounds*, vol. 866, 2021, Art. no. 158783.

[16] K. S. Siow, "Are sintered silver joints ready for use as interconnect material in microelectronic packaging?," *J. Electron. Mater.*, vol. 43, pp. 947–961, 2014.

[17] J. G. Bai, Z. Z. Zhang, J. N. Calata, and G.-Q. Lu, "Low-temperature sintered nanoscale silver as a novel semiconductor device-metallized substrate interconnect material," *IEEE Trans. Compon. Packag. Technol.*, vol. 29, no. 3, pp. 589–593, Sep. 2006.

[18] H. Nishikawa, X. Liu, X. Wang, A. Fujita, N. Kamada, and M. Saito, "Microscale Ag particle paste for sintered joints in high-power devices," *Mater. Lett.*, vol. 161, pp. 231–233, 2015.

[19] E. Ide, A. Hirose, and K. Kobayashi, "Influence of bonding condition on bonding process using Ag metallo-organic nanoparticles for high temperature lead-free packaging," *Mater. Trans.*, vol. 47, pp. 211–217, 2006.

[20] P. Zhang, R. Wei, J. Zeng, M. Cai, J. Xiao, and D. Yang, "Thermal properties of silver nanoparticle sintering bonding paste for high-power LED packaging," *J. Nanomater.*, vol. 2016, 2016, Art. no. 8681513, doi: 10.1155/2016/8681513.

[21] S. Yao et al., "Microscopic investigation on sintering mechanism of electronic silver paste and its effect on electrical conductivity of sintered electrodes," *J. Mater. Sci., Mater. Electron.*, vol. 29, pp. 18540–18546, 2018.

[22] K. Suganuma, S. Sakamoto, N. Kagami, D. Wakuda, K.-S. Kim, and M. Nogi, "Low-temperature low-pressure die attach with hybrid silver particle paste," *Microelectronics Rel.*, vol. 52, no. 2, pp. 375–380, 2012.

[23] B.-G. Park, K.-H. Jung, and S.-B. Jung, "Fabrication of the hybrid Ag paste combined by Ag nanoparticle and micro Ag flake and its flexibility," *J. Alloys Compounds*, vol. 699, pp. 1186–1191, 2017.

[24] S. Wang et al., "Interfacial fracture toughness of sintered hybrid silver interconnects," *J Mater. Sci.*, vol. 55, pp. 2891–2904, 2020.

[25] C. Chen et al., "Robust bonding and thermal-stable Ag–Au joint on ENEPIG substrate by micron-scale sinter Ag joining in low temperature pressure-less," *J. Alloys Compounds*, vol. 828, 2020, Art. no. 154397.

[26] Z. Zhang et al., "Low-temperature and pressureless sinter joining of Cu with micron/submicron Ag particle paste in air," *J. Alloys Compounds*, vol. 780, pp. 435–442, 2019.

[27] C. Chen et al., "Necking growth and mechanical properties of sintered Ag particles with different shapes under air and N_2 atmosphere," *J. Mater. Sci.*, vol. 54, pp. 13344–13357, 2019.

[28] W. Li et al., "Pressureless sinter-joining of micron-Ag flake pastes at 160 °C enabled by solvent and interface engineering," *J. Mater. Process. Technol.*, vol. 322, 2023, Art. no. 118207.

[29] C. Chen et al., "High-temperature reliability of sintered microporous Ag on electroplated Ag, Au, and sputtered Ag metallization substrates," *J. Mater. Sci., Mater. Electron.*, vol. 29, pp. 1785–1797, 2018.

[30] H. Zhan et al., "Silver frameworks based on self-sintering silver microflakes and its application in low temperature curing conductive pastes," *J. Mater. Sci., Mater. Electron.*, vol. 30, pp. 21343–21354, 2019.

[31] R. Luo et al., "Long-time reliable direct bonding of silver flake paste on Al substrate for power electronic die-attachment," *Mater. Lett., X*, vol. 13, 2022, Art. no. 100124.

[32] S. Y. Zhao et al., "Effect of silver flakes in silver paste on the joining process and properties of sandwich power modules (IGBTs Chip/silver paste/Bare Cu)," *J. Electron. Mater.*, vol. 45, pp. 5789–5799, 2016.

[33] Z. Zhang et al., "Enhancement of bonding strength in Ag sinter joining on Au surface finished substrate by increasing Au grain-size," *Appl. Surf. Sci.*, vol. 485, pp. 468–475, 2019.

[34] B. Whitaker et al., "A high-density, high-efficiency, isolated on-board vehicle battery charger utilizing silicon carbide power devices," *IEEE Trans. Power Electron.*, vol. 29, no. 5, pp. 2606–2617, May 2014, doi: 10.1109/TPEL.2013.2279950.

[35] X. She, A. Q. Huang, Ó. Lucía, and B. Ozpineci, "Review of silicon carbide power devices and their applications," *IEEE Trans. Ind. Electron.*, vol. 64, no. 10, pp. 8193–8205, Oct. 2017.

[36] R. A. Wood and T. E. Salem, "Evaluation of a 1200-V, 800-A all-SiC dual module," *IEEE Trans. Power Electron.*, vol. 26, no. 9, pp. 2504–2511, Sep. 2011.

[37] L. Wang et al., "Cu clip-bonding method with optimized source inductance for current balancing in multichip SiC MOSFET power module," *IEEE Trans. Power Electron.*, vol. 37, no. 7, pp. 7952–7964, Jul. 2022.

[38] L. Zhang, X. Yuan, X. Wu, C. Shi, J. Zhang, and Y. Zhang, "Performance evaluation of high-power SiC MOSFET modules in comparison to Si IGBT modules," *IEEE Trans. Power Electron.*, vol. 34, no. 2, pp. 1181–1196, Feb. 2019.

[39] J. Fabre, P. Ladoux, and M. Piton, "Characterization and implementation of dual-SiC MOSFET modules for future use in traction converters," *IEEE Trans. Power Electron.*, vol. 30, no. 8, pp. 4079–4090, Aug. 2015.

[40] Y. Hinata, M. Horio, Y. Ikeda, R. Yamada, and Y. Takahashi, "Full SiC power module with advanced structure and its solar inverter application," in *Proc. 28th Annu. IEEE Appl. Power Electron. Conf. Expo.*, 2013, pp. 604–607.

[41] Y. Zhang, H.-P. Nee, T. Hammam, I. Belov, P. Ranstad, and M. Bakowski, "Multiphysics characterization of a novel SiC power module," *IEEE Trans. Compon., Packag. Manuf. Technol.*, vol. 9, no. 3, pp. 489–501, Mar. 2019.

[42] A. Osman, G. Moreno, S. Myers, S. V. J. Narumanchi, and Y. Joshi, "Single-Phase jet impingement cooling for a power-dense silicon carbide power module," *IEEE Trans. Compon., Packag. Manuf. Technol.*, vol. 13, no. 5, pp. 615–627, May 2023.

[43] K. Sugiura et al., "Reliability evaluation of SiC power module with sintered Ag die attach and stress-relaxation structure," *IEEE Trans. Compon., Packag. Manuf. Technol.*, vol. 9, no. 4, pp. 609–615, Apr. 2019.

[44] Z. Chen and A. Q. Huang, "High performance SiC power module based on repackaging of discrete SiC devices," *IEEE Trans. Power Electron.*, vol. 38, no. 8, pp. 9306–9310, Aug. 2023.

[45] Z. Liang, P. Ning, and F. Wang, "Development of advanced all-SiC power modules," *IEEE Trans. Power Electron.*, vol. 29, no. 5, pp. 2289–2295, May 2014.

[46] J. Li, A. Castellazzi, M. A. Eleffendi, E. Gurpinar, C. M. Johnson, and L. Mills, "A physical RC network model for electrothermal analysis of a multichip SiC power module," *IEEE Trans. Power Electron.*, vol. 33, no. 3, pp. 2494–2508, Mar. 2018.

[47] T. G. Lei, J. N. Calata, G.-Q. Lu, X. Chen, and S. Luo, "Low-temperature sintering of nanoscale silver paste for attaching large-area (>100 mm2) chips," *IEEE Trans. Compon. Packag. Technol.*, vol. 33, no. 1, pp. 98–104, Mar. 2010.

[48] C. Chen et al., "Bonding technology based on solid porous Ag for large area chips," *Scripta Materialia*, vol. 146, pp. 123–127, 2018.

[49] C. Choe, C. Chen, S. Noh, and K. Suganuma, "Thermal shock performance of DBA/AMB substrates plated by Ni and Ni–P layers for high-temperature applications of power device modules," *Materials*, vol. 11, no. 12, 2018, Art. no. 2394.

[50] D. Kim, C. Chen, S. Nagao, and K. Suganuma, "Mechanical characteristics and fracture behavior of GaN/DBA die-attached during thermal aging: Pressure-less hybrid Ag sinter joint and Pb–5Sn solder joint," *J. Mater. Sci., Mater. Electron.*, vol. 31, pp. 587–598, 2020.

[51] C. Chen et al., "Interface-mechanical and thermal characteristics of Ag sinter joining on bare DBA substrate during aging, thermal shock and 1200 W/cm2 power cycling tests," *IEEE Trans. Power Electron.*, vol. 37, no. 6, pp. 6647–6659, Jun. 2022.

[52] C. Chen and K. Suganuma, "Microstructure and mechanical properties of sintered Ag particles with flake and spherical shape from nano to micro size," *Mater. Des.*, vol. 162, pp. 311–321, 2019.

[53] J. Yeom et al., "Ag particles for sinter bonding: Flakes or spheres?," *Appl. Phys. Lett.*, vol. 114, 2019, Art. no. 253103, doi: 10.1063/1.5099140.

[54] H. Zhang et al., "Enhancing low-temperature and pressureless sintering of micron silver paste based on an ether-type solvent," *J. Electron. Mater.*, vol. 46, pp. 5201–5208, 2017.

[55] Y. Liu et al., "Development of crack-less and deformation-resistant electroplated Ni/electroless Ni/Pt/Ag metallization layers for Ag-sintered joint during a harsh thermal shock," *Mater. Des.*, vol. 224, 2022, Art. no. 111389.

[56] D. Kim, Y. Yamamoto, S. Nagao, N. Wakasugi, C. Chen, and K. Suganuma, "Measurement of heat dissipation and thermal-stability of power modules on DBC substrates with various ceramics by SiC micro-heater chip system and Ag sinter joining," *Micromachines*, vol. 10, no. 11, p. 745, 2019, doi: 10.3390/mi10110745.

[57] S. F. Choudhury and L. Ladani, "Local shear stress-strain response of Sn-3.5Ag/Cu solder joint with high fraction of intermetallic compounds: Experimental analysis," *J. Alloys Compounds*, vol. 680, pp. 665–676, 2016.

[58] P. Šebo et al., "The influence of silver content on structure and properties of Sn-Bi-Ag solder and Cu/solder/Cu joints," *Mater. Sci. Eng. A*, vol. 571, pp. 184–192, 2013.

[59] H. Zhang, C. Chen, J. Jiu, S. Nagao, and K. Suganuma, "High-temperature reliability of low-temperature and pressureless micron Ag sintered joints for die attachment in high-power device," *J. Mater. Sci., Mater. Electron.*, vol. 29, pp. 8854–8862, 2018.

[60] S. A. Paknejad and S. H. Mannan, "Review of silver nanoparticle based die attach materials for high power/temperature applications," *Microelectronics Rel.*, vol. 70, pp. 1–11, 2017.

[61] H. S. Chin, K. Y. Cheong, and A. B. Ismail, "A review on die attach materials for SiC-based high-temperature power devices," *Metall. Mater. Trans. B*, vol. 41, no. 4, pp. 824–832, 2010.

[62] K. Asama, T. Matsuda, T. Ogura, T. Sano, M. Takahashi, and A. Hirose, "Low-temperature metal-to-alumina direct bonding process utilizing redox reaction between silver oxide and organic agent," *Mater. Sci. Eng., A*, vol. 702, pp. 398–405, 2017.

[63] Y. Zhou, L. Xu, and S. Liu, "Optimization for warpage and residual stress due to reflow process in IGBT modules based on pre-warped substrate," *Microelectronic Eng.*, vol. 136, pp. 63–70, 2015.

[64] G. Mirone, A. Sitta, G. D'Arrigo, and M. Calabretta, "Material characterization and warpage modeling for power devices active metal brazed substrates," *IEEE Trans. Device Mater. Rel.*, vol. 19, no. 3, pp. 537–542, Sep. 2019.

[65] Y. Tan, X. Li, G. Chen, Q. Gao, G. Lu, and X. Chen, "Effects of thermal aging on long-term reliability and failure modes of nano-silver sintered lap-shear joint," *Int. J. Adhesion Adhesives*, vol. 97, 2020, Art. no. 102488.

[66] P. Gadaud, V. Caccuri, D. Bertheau, J. Carr, and X. Milhet, "Ageing sintered silver: Relationship between tensile behavior, mechanical properties and the nanoporous structure evolution," *Mater. Sci. Eng., A*, vol. 669, pp. 379–386, 2016.

[67] S. Ramminger, N. Seliger, and G. Wachutka, "Reliability model for Al wire bonds subjected to heel crack failures," *Microelectronics Rel.*, vol. 40, no. 8–10, pp. 1521–1525, 2000.

[68] J. Onuki, M. Koizumi, and M. Suwa, "Reliability of thick Al wire bonds in IGBT modules for traction motor drives," *IEEE Trans. Adv. Packag.*, vol. 23, no. 1, pp. 108–112, Feb. 2000.

[69] C. Choe, C. Chen, S. Nagao, and K. Suganuma, "Real-time acoustic emission monitoring of wear-out failure in SiC power electronic devices during power cycling tests," *IEEE Trans. Power Electron.*, vol. 36, no. 4, pp. 4420–4428, Apr. 2021.

[70] S. A. Paknejad, G. Dumas, G. West, G. Lewis, and S. H. Mannan, "Microstructure evolution during 300°C storage of sintered Ag nanoparticles on Ag and Au substrates," *J. Alloys Compounds*, vol. 617, pp. 994–1001, 2014.

[71] C. Chen, "Effect of oxygen on microstructural coarsening behaviors and mechanical properties of Ag sinter paste during high-temperature storage from macro to micro," *J. Alloys Compounds*, vol. 834, 2020, Art. no. 155173.

[72] K. S. Siow and S. T. Chua, "Thermal ageing studies of sintered micron-silver (Ag) joint as a lead-free bonding material," *Met. Mater. Int.*, vol. 26, pp. 1404–1414, 2020.

[73] F. Yu, J. Cui, Z. Zhou, K. Fang, R. W. Johnson, and M. C. Hamilton, "Reliability of Ag sintering for power semiconductor die attach in high-temperature applications," *IEEE Trans. Power Electron.*, vol. 32, no. 9, pp. 7083–7095, Sep. 2017.

[74] D. Kim et al., "Fracture mechanism of microporous Ag-sintered joint in a GaN power device with Ti/Ag and Ni/Ti/Ag metallization layer at different thermo-mechanical stresses," *J. Mater. Sci.*, vol. 56, pp. 9852–9870, 2021.

[75] D. Kim et al., "Development of high-strength and superior thermal shock-resistant GaN/DBA die attach structure with Ag sinter joining by thick Ni metallization," *Microelectronics Rel.*, vol. 100/101, 2019, Art. no. 113380.

[76] D. Kim et al., "Strengthening of DBA substrate with Ni/Ti/Ag metallization for thermal fatigue-resistant Ag sinter joining in GaN power modules," *J. Mater. Sci., Mater. Electron.*, vol. 31, pp. 3715–3726, 2020.

[77] A. Kunwar et al., "Heat and mass transfer effects of laser soldering on growth behavior of interfacial intermetallic compounds in Sn/Cu and Sn-3.5Ag0.5/Cu joints," *Microelectronics Rel.*, vol. 80, pp. 55–67, 2018.

[78] A. Tan and F. Yusof, "Influence of nanoparticle addition on the formation and growth of intermetallic compounds (IMCs) in Cu/Sn–Ag–Cu/Cu solder joint during different thermal conditions," *Sci. Technol. Adv. Mater.*, vol. 16, no. 3, 2015, Art. no. 033505.